DOE/JPL/954868-3

AUTOMATED ARRAY ASSEMBLY, PHASE II

Quarterly Report No. 3, April 1—June 30, 1978

By
R. V. D'Aiello

June 1978

Work Performed Under Contract No. NAS-7-100-954868

RCA Laboratories
Princeton, New Jersey

U.S. Department of Energy

Solar Energy

DISCLAIMER

NOTICE

DRL Line Item No. 10

DOE/JPL/954868-3
Distribution Category UC-63b

AUTOMATED ARRAY ASSEMBLY, PHASE II

R. V. D'Aiello
RCA Laboratories
Princeton, New Jersey 08540

QUARTERLY REPORT NO. 3

JUNE 1978

This work was performed for the Jet Propulsion Laboratory, California Institute of Technology, under NASA Contract NAS7-100 for the Department of Energy.

The JPL Low-Cost Silicon Solar Array Project is funded by DOE and forms part of the DOE Photovoltaic Conversion Program to initiate a major effort toward the development of low-cost solar arrays.

Prepared Under Contract No. 954868 For

JET PROPULSION LABORATORY
CALIFORNIA INSTITUTE OF TECHNOLOGY
Pasadena, California 91103

THIS PAGE

WAS INTENTIONALLY

LEFT BLANK

PREFACE

This Quarterly Report, prepared by RCA Laboratories, Princeton, NJ 08540 describes the results of work performed from April 1, 1978 to June 30, 1978 in the Energy Systems Research Laboratory, B. F. Williams, Director; Materials and Process Laboratory, Solid State Division, Somerville, NJ, H. Veloric, Manager; and at the Advanced Technology Laboratory, Government and Commercial Systems, Camden, NJ, F. E. Shashoua, Director. The Project Scientist is R. V. D'Aiello and the Project Supervisor is D. Richman, Head, Semiconductor Materials Research. Others who participated in the research and writing of this report are:

J. Toner	-	cost analysis
D. Richman	-	silicon material
G. Schnable	-	metallization and AR coating
W. Kern	-	
K. Bube	-	
R. Scott	-	panel design and fabrication
M. Crouthamel	-	
H. Veloric	-	manufacturing
F. Mayer	-	
U. Roundtree	-	
L. Guarino	-	

The JPL Task Manager is Don Bickler.

TABLE OF CONTENTS

LIST OF ILLUSTRATIONS

LIST OF TABLES

SECTION I

SUMMARY

During this quarter progress has been made in the following areas.

A. ION-IMPLANTED JUNCTION FORMATION AND SOLAR CELLS

An effective boron-glass back-surface gettering process has been reproducibly demonstrated in combination with ion-implanted junctions. Efficiencies of 12 to 15% (AM-1) on 2- x 2-cm solar cells were consistently obtained. The effect on cell performance of variations in the phosphorus dose level from 2×10^{14} to 1×10^{16} A/cm^2 were studied, and a systematic increase in efficiency with dose level was found with a peak in cell performance occurring at a dose of $\sim 5 \times 10^{15}$ A/cm^2. In addition, variations of the present gettering technique and comparisons with other gettering processes have been conducted.

B. SCREEN-PRINTED THICK-FILM METALLIZATION

Materials characterization for solar-cell silver metallization has been continued by comparing the results with commercial and RCA-synthesized inks. Some testing pertaining to solderability, adhesion, and electrical performance has been completed. Penetration studies have been conducted by comparing surface physical damage with n-layer phosphorus concentration profiles by the secondary-ion mass spectroscopy (SIMS) method. Comparative studies of inks and methods of firing including belt furnace and infrared lamp heating have shown some versatility of the process and successful metallizations, good adherence, and solderability with one RCA ink and one commercial ink.

C. SPRAY-ON AR COATINGS

A spray-on antireflection (AR) coating solution has been synthesized which yields TiO_2 films of the required thickness and a refractive index of 2.1. Spraying tests were conducted using the Zicon* model 11,000 autocoater, and AR films were produced with satisfactory thickness and index control. The

*Zicon Corporation, Mount Vernon, NY.

efficiency of typical solar cells (7.5 cm diameter) increased by a factor of 1.4 after application of the AR coating. Preparing our own source concentrate allows full control over composition and materials and results in a substantial cost savings.

D. INTERCONNECT AND PANEL ASSEMBLY

Experiments were performed to demonstrate feasibility of laminating cells with polyvinyl butyral (PVB) and acrylic between two sheets of glass. Panels up to 4- by 4-ft were successfully laminated with PVB. The cell configuration is the same as would be used in a production design, including all interconnects.

A method has been devised by which entire arays of solar cells can be electrically interconnected in a single "mass soldering" process wherein the cells are radiantly heated directly. A 1-ft^2 prototype was constructed, and several nine-cell arrays were produced using this method.

SECTION II

INTRODUCTION

The purpose of our overall program is to establish technological readiness and provide verification for the elements of a manufacturing sequence which would ultimately be suitable for the large-scale production of silicon solar-array modules at a selling price of less than $500/kW. A program and process plan for accomplishing this objective was developed and put into operation during the first quarter. This plan is centered around the processing sequence shown in Fig. 1. Three junction-formation processes are shown; since our cost analysis shows that they do not differ greatly in cost, each should be considered for technical merits and possible future cost reduction. In Section III the progress made in the various process steps of the plan is described, and plans for the next quarter are summarized in Section IV.

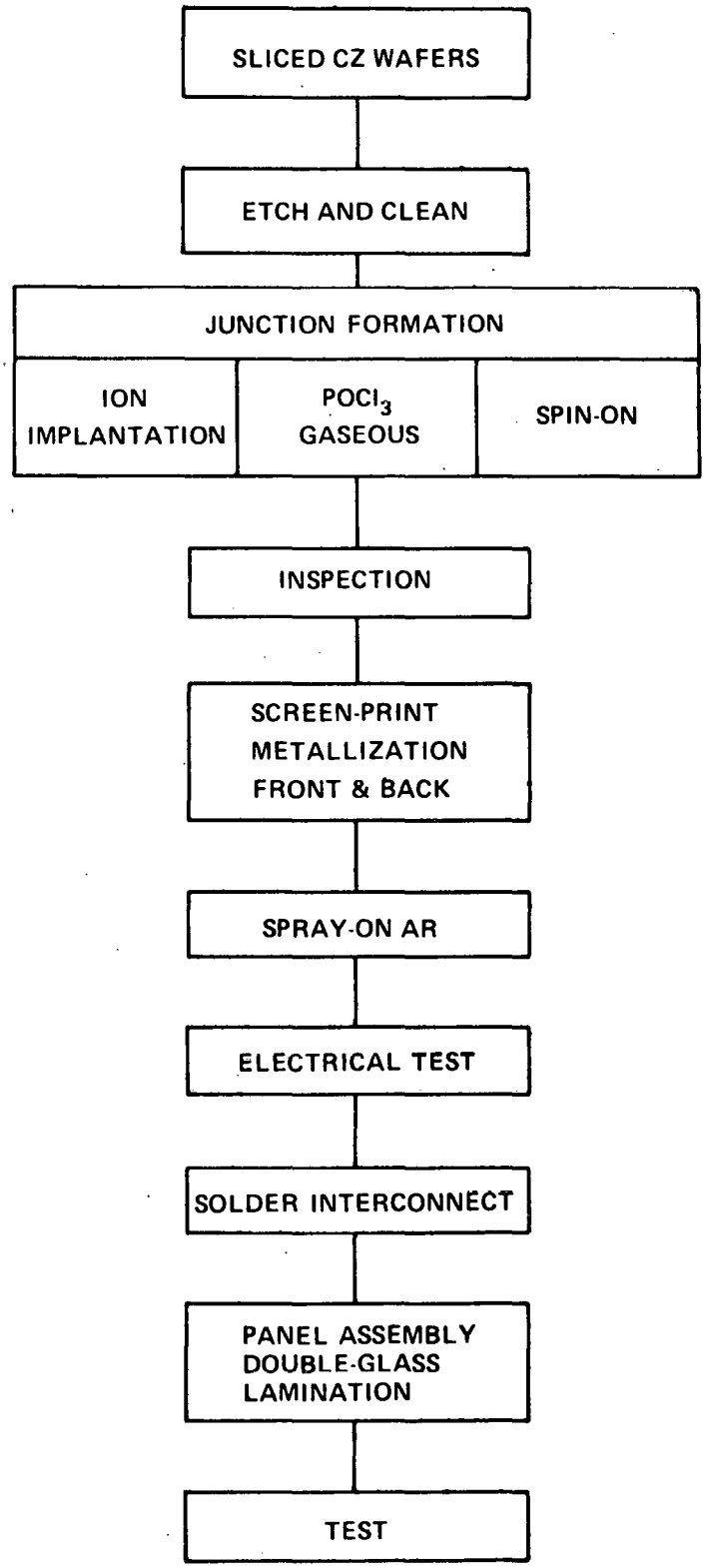

Figure 1. Major steps of process sequence.

SECTION III

PROGRESS

A. JUNCTION FORMATION - SOLAR CELLS

1. Ion Implantation

a. Variation of ^{31}P Dose Level - The results of our studies given in the previous quarterly reports [1,2] have shown that incorporation of a boron-glass backside gettering process significantly increases the efficiencies of the resultant solar cells. After incorporating this gettering step as a standard part of the ion-implantation process, a study was made of a number of cell variables as a function of dose and annealing temperature, at a constant implant energy of 5 keV. The results of a more complete study of the effect of dose variation on cell efficiency and open-circuit voltage are shown in Figs. 2 and 3. Both figures show a systematic increase in cell parameters as a function of dose with a peak in performance occurring at a dose level of about 5×10^{15} A/cm^2.

b. Gettering Techniques - Since gettering plays such an important role in obtaining high-efficiency ion-implanted solar cells, we have investigated the effect of several gettering techniques on cell performance.

The variations of the two basic gettering techniques are shown below:

Boron Glass Back	Three-Step Anneal (^{11}B Back Implant)
900°C - 30 min	550 - 2 h
1000°C - 30 min	850°C - 15 min
	550°C - 2 h

Dose (^{31}P) level variations were included in the test matrix as well as a combination of both gettering techniques as shown in Table 1.

---

1. R. V. D'Aiello, *Automated Array Assembly, Phase II*, Quarterly Report No. 1, prepared under Contrast No. 954868 for Jet Propulsion Laboratory, December 1977.
2. R. V. D'Aiello, *Automated Array Assembly, Phase II*, Quarterly Report No. 2, prepared under Contract No. 954868 for Jet Propulsion Laboratory, March 1978.

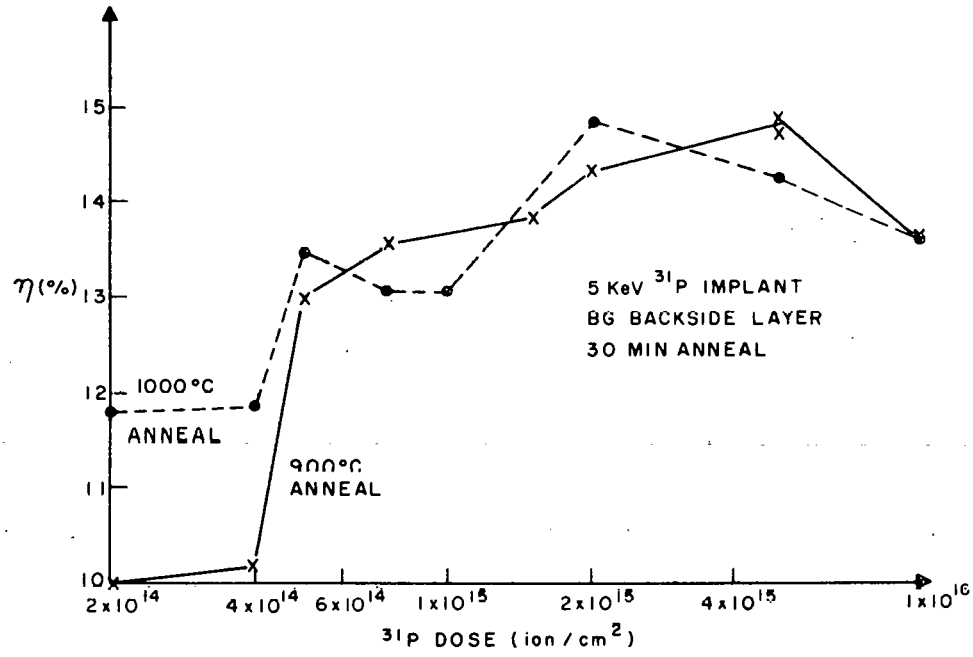

Figure 2. Effect of various ion implants on solar-cell efficiency

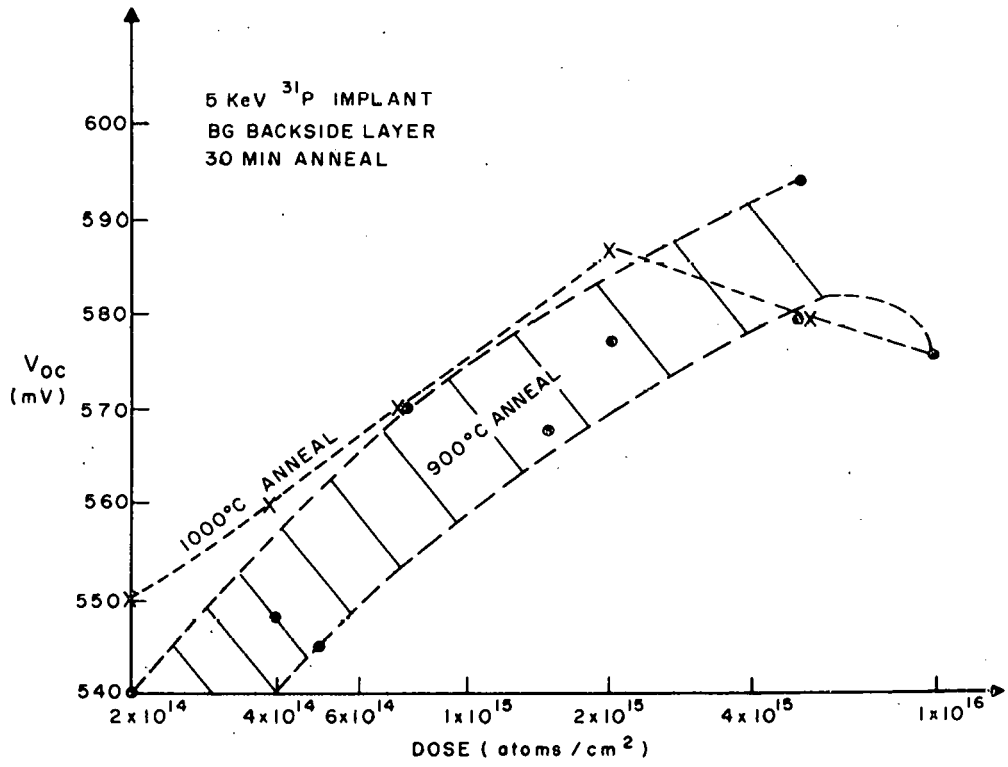

Figure 3. Effect of implant dosage on V_{OC}.

TABLE 1. GETTERING AND DOSE IMPLANT MATRIX

Cell	^{31}P Dose		B^{11}		
-	5×10^{14}	Boron glass backside anneal 900°C for 30 min			
67	1×10^{15}				
68	5×10^{15}				
69	1×10^{16}				
70	5×10^{15}	Boron glass backside anneal 1000°C for 30 min			
71	1×10^{16}				
72	5×10^{14}		5×10^{15}	550°C 2 h 850°C 15 min 550°C 2 h	BC 900°C
74, 75	1×10^{15}		5×10^{15}		
76	5×10^{15}		5×10^{15}		
- - - -	- - - - -				
78, 79	5×10^{14}				
80, 81	1×10^{15}				
83	5×10^{15}				

Boron-Gettering Sequence

1. SC1, SC2 clean
2. Boron deposition at 800°C
3. Anneal as follows:

Wafers	Temp	Time Followed by 10-min slow cooling
66, 67, 68, 69 78, 79, 80, 81, 82, 83	900°C	25
70, 71	1000°C	25
72 to 77	no boron-glass gettering step	

The results of this test are given in Table 2. It can be seen that while the three-step technique yields reasonably good cell parameters at the higher dose levels, the boron-gettering process either alone or in combination with the three-step heating cycle results in higher cell efficiency at all dose levels. The general trend of increased cell performance with dose level peaking at $\sim 5 \times 10^{15}$ A/cm^2 is somewhat more pronounced for the three-step gettering case.

TABLE 2. SUMMARY OF RESULTS FOR ION-IMPLANTED SOLAR CELLS WITH DIFFERENT GETTERING TECHNIQUES

			AM-1 Parameters			
Sample	^{31}P Dose (A/cm^2)	Gettering Process	J_{sc}^{+} (mA/cm^2)	V_{oc} (mV)	F. F. -	η (%)
67	1E15	Boron glass, 900°C, 30 min	30.5	575	0.771	13.5
68	5E15	Boron glass, 900°C, 30 min	30.2	580	0.752	13.2
69	1E16	Boron glass, 900°C, 30 min	29.9	575	0.772	13.3
70	5E15	Boron glass, 1000°C, 30 min	29.2	577	0.780	13.1
71	1E16	Boron glass, 1000°C, 30 min	29.6	575	0.780	13.3
72	5E14	550°C, 2h / 850°C, 15 min / 550°C, 2 h	28.0	567	0.686	10.9
74	1E15		28.6	558	0.755	12.1
75	1E15		29.2	567	0.771	12.8
76	5E15		29.8	574	0.778	13.3
78	5E14	550°C, 2h / 850°C, 15 min / 550°C, 2h + BG 900°C 30 min	31.2	572	0.760	13.6
79	5E14		31.2	575	0.752	13.5
80	1E15		30.5	565	0.753	13.0
81	1E15		30.6	566	0.750	13.0
83	5E15		31.7	591	0.781	14.6

2. Liquid Dopant Sources

We have completed a test comparing alcohol- and aqueous-based phosphorus liquid dopant sources.* Solar cells of 4.4 cm^2 area were fabricated on several different starting wafers. The liquids were spun-on, and a basic junction

*Purchased from Emulsitone Company, Whippany, NJ.

anneal was done at 850°C for 50 min followed by two different anneal schedules for each dopant base. The results of this test are shown in Table 3.

TABLE 3. RESULTS OF A COMPARISON OF ALCOHOL- AND AQUEOUS-BASED PHOSPHORUS DOPANTS

Sample	Wafer ρ (Ω-cm)	P Dopant Base	Junction	Anneal	AM-1 Parameters J_{sc} (mA/cm^2)	V_{oc} (mV)	F.F. -	η (%)
3A	1-2	Alcohol	850°C 50 min	600°C 120 min	29.6	490	0.40	5.8
5B-20	1-2	Aqueous	850°C 50 min	600°C 120 min	30.8	575	0.76	13.4
2A-20	1-2	Alcohol	850°C 50 min	10 min Slow pull	29.0	500	0.55	8.0
5B	1-2	Aqueous	850°C 50 min	10 min Slow pull	30.7	580	0.77	13.7
9A	8-15	Alcohol	850°C 50 min	600°C 120 min	31.0	540	0.42	7.0
12B	8-15	Aqueous	850°C 50 min	600°C 120 min	26.7	557	0.77	11.4
16B	5	Aqueous	850°C 50 min	600°C 120 min	31.6	570	0.79	14.2

The results clearly show that under the anneal conditions used in this test, superior junction characteristics and solar-cell performance were obtained with the aqueous-based phosphorus source when compared with the alcohol-based liquid.

In addition, in separate tests it was shown that the aqueous-based liquids can be rolled or screened onto the wafers with satisfactory coverage and resultant junction quality.

We also began a similar study of arsenic sources. Alcohol-based arsenic was used in these initial tests. Since arsenic diffuses considerably slower than phosphorus, the diffusions were done at 1000°C for 60 min as compared with 850°C for 50 min for phosphorus. Typical results for solar cells fabricated using the spin-on arsenic source are given in Table 4.

Generally, poor junctions were formed, resulting in low values of open-circuit voltage and fill factor. Also, no correlation was noted with annealing conditions or back-surface boron application. The listed short-circuit

TABLE 4. CHARACTERISTICS OF SOLAR CELLS MADE WITH SPIN-ON, ALCOHOL-BASED ARSENIC SOURCE

Sample No.	Wafer ρ (Ω-cm)	Junction Formation		Spin-on Boron on Back		AM-1 Parameters			
		Diffusion	Anneal	Yes	No	J_{sc} (mA/cm^2)	V_{oc} (mV)	F.F. -	η (%)
51	1-3	1000°C 60 min	Slow cool to 800°C		✓	17.3	437	0.46	3.5
53	1-3	1000°C 60 min	10 min Slow pull		✓	24.6	516	0.57	7.3
55	1-3	1000°C 60 min	Slow cool to 800°C	✓		23.3	517	0.75	9.0
57	1-3	1000°C 60 min	10 min Slow pull	✓		24.7	470	0.63	7.3

currents are considerably lower than those obtained with the use of liquid phosphorus sources. A comparison of the spectral responses for two cells made with arsenic and phosphorus sources (Fig. 4) shows that the red response is much lower for the arsenic source, indicating that low diffusion length was obtained. From these tests, it is not clear whether this is due to the use of the alcohol-based arsenic or to the higher processing temperature. Tests using aqueous-based arsenic are planned.

B. SCREEN-PRINTED METALLIZATION

1. Solderability and Adhesion

To determine relative solderability and adhesion strength values, we performed some preliminary tests. Both OI-6105* phosphated-silver ink and RCA-inks were screened onto 96% Al_2O_3 substrates using the 1874-square serpentine pattern. After drying and firing for 10 min at 675°C, the metallization patterns were coated with Kester 1544** solder flux and immersed in 215°C solder, i.e., 62Sn-36Pb-2Ag (wt pct), for varying times from 2 to 8 s. The sample patterns were visually examined to determine the extent of solder

*Owens-Illinois, Inc., Toledo, OH.
**Kester Solder Co., Chicago, IL.

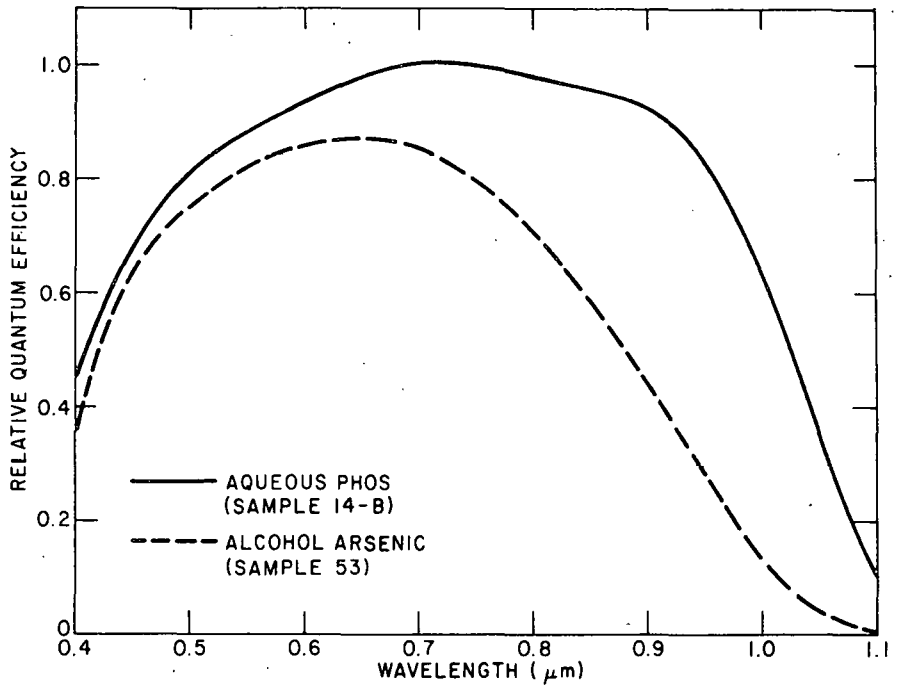

Figure 4. Comparison of spectral responses for cells made with phosphorus and arsenic liquid sources.

dewetting which is indicative of excessive silver dissolution by the solder or poor initial wettability. As shown in Table 5, OI-6105 is essentially unsolderable or too rapidly dissolved by the solder. The first RCA ink, e.g., Metz* FS type C Ag + 10 vol pct PBS frit [i.e., $80PbO\text{-}10B_2O_3\text{-}10SiO_2$ (wt pct)] showed only slight dewetting up to 5 s. The second RCA ink, e.g., Metz FS type C Ag + 10 vol pct PBS frit + 3 wt pct Al, showed slightly greater dewetting but more resistance to longer immersion in molten solder.

Despite the poor solderability of OI-6105 it was included in the adhesion strength determinations which followed. The two RCA Ag inks, frit-bearing Engelhard** 422E (Ag) and 422F (Ag/Al), and Thick Film Systems† (TFS) 3347 (Ag) were also included, as well as fritless Thick Films Systems 250 (Ag). All the inks were screen-printed onto polished (100) silicon substrates to yield four test pads measuring 0.1- x 0.1-in. (2.5- x 2.5-mm) square. The samples were dried and fired under three separate conditions: (A) 675°C for 2 min in a

*Metz Metallurgical Co., South Plainfield, NJ.
**Engelhard Industries, East Newark, NJ.
†Thick Film Systems, Inc., Santa Barbara, CA.

TABLE 5. SOLDERABILITY COMPARISON - PERCENT DEWETTING

Metallization	Time (s) in 215°C - Solder (62Sn-36Pb-2Ag, wt pct)*			
	8	6	4	2
OI-6105	70-80	80-85	70-80	70-80
RCA-Metz FS Type C+ 10 vol pct PBS**	30-40	1	2	1
RCA-Metz FS Type C+ 10 vol pct PBS** +3 wt pct Al	5	5	5	5

*Flux: Kester 1544
**Frit: PBS is $80PbO-10B_2O_3-10SiO_2$ (wt pct)

tube furnace, (B) 675°C for 5 min in a belt furnace moving at 15.2 cm (6 in.)/min, and (C) 675°C for 10 min in the belt furnace moving at 7.6 cm (3 in.)/min. Copper straps were then applied by a reflow soldering technique for adhesion shear stress testing. The copper straps, which were pretinned with solder, measured 1.34 x 0.14 x 0.003 in. (34 x 3.5 x 0.08 mm). Kester 1544 solder flux and two 62Sn-36Pb-2Ag solder balls weighing about 0.005 g each were applied to the metallization test pads. The copper straps were positioned over the test pads, and the assembly was placed on a 215 $\pm$2°C hot plate. Heating to 215°C took about 45 s, and the assembly was held at 215°C for 5 to 8 s before quickly removing and cooling on a chilling block.

A shearing stress was then applied to the copper strap-metallization interface in an Instron* Test Machine after allowing the assemblies to equilibrate for several hours at room temperature. The shearing forces, reported in Table 6, indicate a range of 0 (TFS fritless Ag 250) to 608 g value is equivalent to 1342 lb/in.^{2} (0.94 kg/mm^2) shear stress over the entire pad area. In many instances, however, the copper strap broke, in which case the silicon-metallization interface failure stress was not actually achieved, i.e., the interface strength exceeded the copper strap strength. In general, the three failure modes, e.g., copper, silicon, and interface

*Instron Corp., Canton, MA.

TABLE 6. METALLIZATION ADHESION SUMMARY FIRING CONDITIONS

Ink	Parameter	A 675°C-2 min (Tube)	B 675°C-5 min (Belt-6 in./min)	C 675°C-10 min (Belt-3 in./min)
OI-6105	$\bar{x}$* (g)	-	4015	4045
	%V**	-	33.3	8.7
	mode+	-	b	a,b,c
TFS 3347	$\bar{x}$	0	2775	0
	%V		21.7	
	mode	c	c	c
TFS 3347	$\bar{x}$ (g)	5465	5823	4818
	%V	9.1	5.3	11.9
	mode	a,b	a	a
Eng 422E	$\bar{x}$ (g)	0	4460	3930
	%V		43.3	37.8
	mode	c	b,c	a,b,c
Eng 422F	$\bar{x}$ (g)	3310	4218	3828
	%V	35.6	14.4	16.7
	mode	c	c	a,b,c
RCA-Metz FS Type C + 10 vol pct PBS	$\bar{x}$ (g)	4785	6015	5443
	%V	2.6	7.4	3.2
	mode	b,c	a	a
RCA-Metz FS Type C + 10 vol pct PBS + 3 wt pct Al	$\bar{x}$ (g)	4785	5533	5443
	%V	3.2	8.2	27.6
	mode	a,b	a,b	a,b

*$\bar{x}$ = shearing force, average value.
**%V = coefficient of variation.
+ Legend for failure mode: a = copper strap broke
b = silicon wafer broke partially or completely.
c = delamination somewhere between copper strap and silicon.

failure, were observed on various inks with the weaker ones showing a predominance of interface failures. The stronger inks are generally noted to be the RCA inks and TFS 3347.

2. Powder Characterization

The Al and three Ag powders were analyzed by the x-ray sedimentation technique to illustrate the wide differences in particle size distribution and to further characterize the successfully utilized Metz FS Type C Ag and U.S. Bronze* Ampal 631 Al. Whereas the Metz K-150 Ag has a median particle size of 4 μm, as shown in Fig. 5, which is identical to Metz FS Type C, the former contains a greater percentage of smaller particles. While smaller particles may be beneficial in achieving more rapid sintering at lower temperatures, greater vehicle content is necessary in making a printable ink. This requirement effectively lowers metal content which in turn adversely affects line conductivity. Consequently, the useful Ag powders will more closely approximate the particle size distribution curve of Metz FS Type C. In the case of Al powder a coarser particle size distribution is needed to minimize excessive oxidation, either initially in powder preparation or during firing. It is not known how fine an Al powder can be before excessive oxidation becomes problematical in this application. However, at this point the Al powder appears to be adequate.

3. Metallization Penetration

The range of phosphorus concentration profiles for eight lots of Somerville-diffused junctions are shown in Fig. 6. Since it is known that metallization contact resistance rises abruptly if the phosphorus concentration is much below 10^{19} A/cm^2, it is apparent, from Fig. 6, that metallization penetration, i.e., dissolution of the high phosphorus concentration region by ink constituents, must be less than about 0.1 μm average. If nominal junction depths are less than 0.55 μm, the permissible penetration may be considerably less than 0.1 μm. Consequently, some microscopic and SEM techniques were employed to determine the extent of penetration on (100) and (111) Si surfaces. For this initial test,

*U.S. Bronze, Inc., Flemington, NJ.

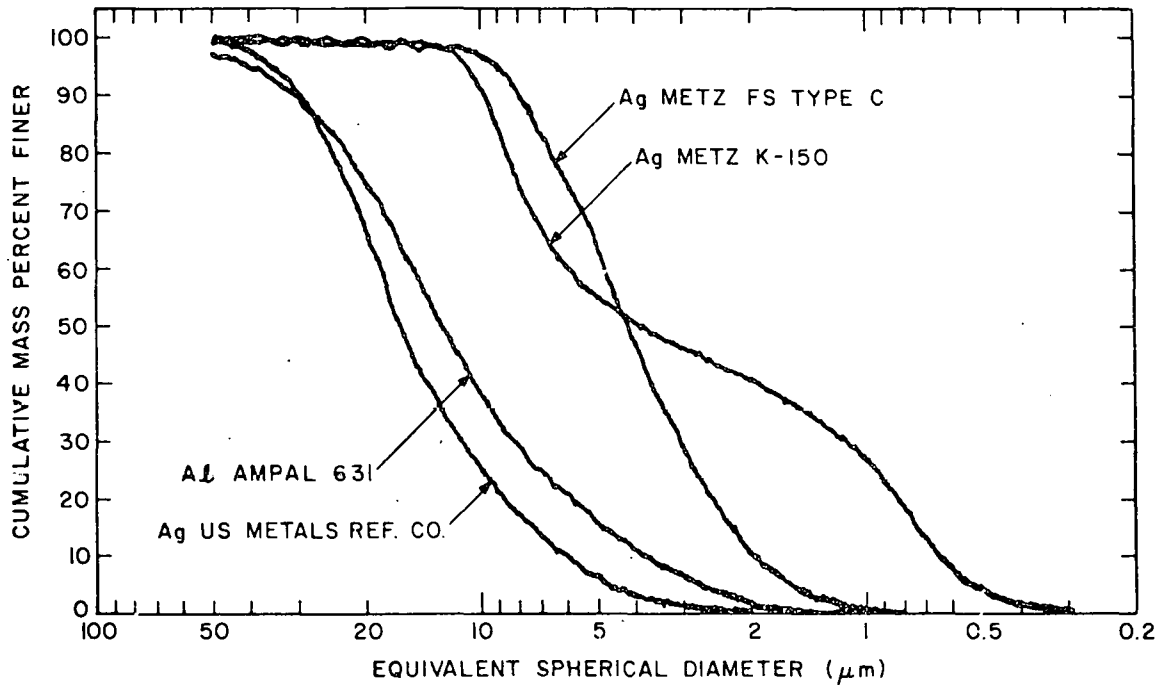

Figure 5. Powder particle size distribution curves.

0.55-μm-junction-depth (100) silicon solar-cell material was compared with nominally 100-Ω-cm (111) silicon. RCA-Metz FS Type C + 10 vol pct $AgPO_3$ metallization was screen printed onto samples of both crystallographic orientations and fired for 2 min at 650°C and 10 min at 700°C in a tube furnace. Subsequently, the Ag was removed by etching in 1:1 NH_4OH-H_2O_2 solution and the $AgPO_3$ was dissolved in concentrated HF. The surfaces were then immersed in Sirtl etch (40HF-40H_2O-3.3 g CrO_3) for 1 min.

As shown by Nomarksi differential interference contrast microscopy in Fig. 7, both 650°C-2 min-fired crystallographic orientations appear to have been attacked by the metallization. In the n-layered (100) Si, however, additional peripheral attack is noted. This attack is believed to be the result of more highly concentrated $AgPO_3$ in that region. The $AgPO_3$ spreads laterally on the Si surface after first wetting the Si immediately beneath the printed pattern. The tendency to wet Si results in a net loss of $AgPO_3$ in the metallized area with a corresponding increase in concentration at the periphery of the deposit. As shown in Fig. 8 the attack in both materials is more vigorous when fired at 700°C for 10 min. From the SEM photographs in Fig. 9, the actual attack of the Si by dissolving in $AgPO_3$ after 10 min at

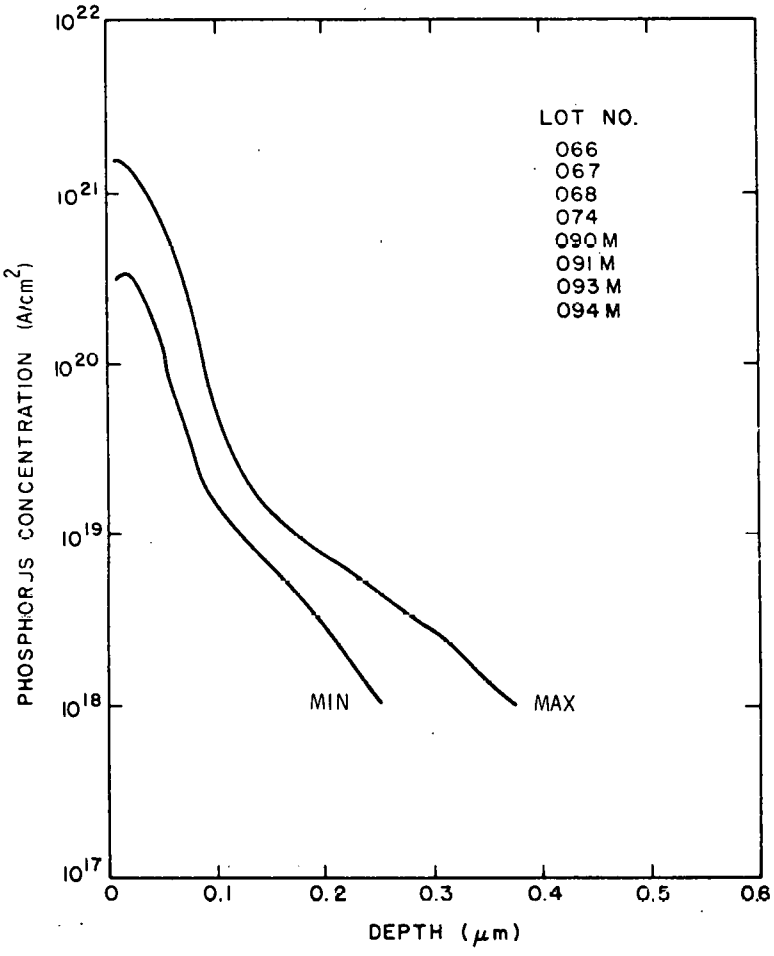

Figure 6. Range of $POCl_3$-diffused phosphorus concentration profiles.

700°C is on the order of 0.1 μm in isolated spots. Alternatively, the Si can be dissolved in the solid state by Ag, provided by the metal powder or chemically reduced $AgPO_3$. In localized spots this could result in shunting in the p-Si, if ohmic contact is formed. Clearly, the Si attack must be minimized by decreasing the time-temperature product, if shallower n-layers are to be used. If the penetration is proportional to $(Dt)^{1/2}$, it may be adequately minimized by shorter times at higher temperatures or longer times at lower temperatures without raising the Ag resistivity significantly. To this end, infrared heating, which provides a rapid rise in temperature, should be able to accomplish the required short-time-high-temperature combination while also

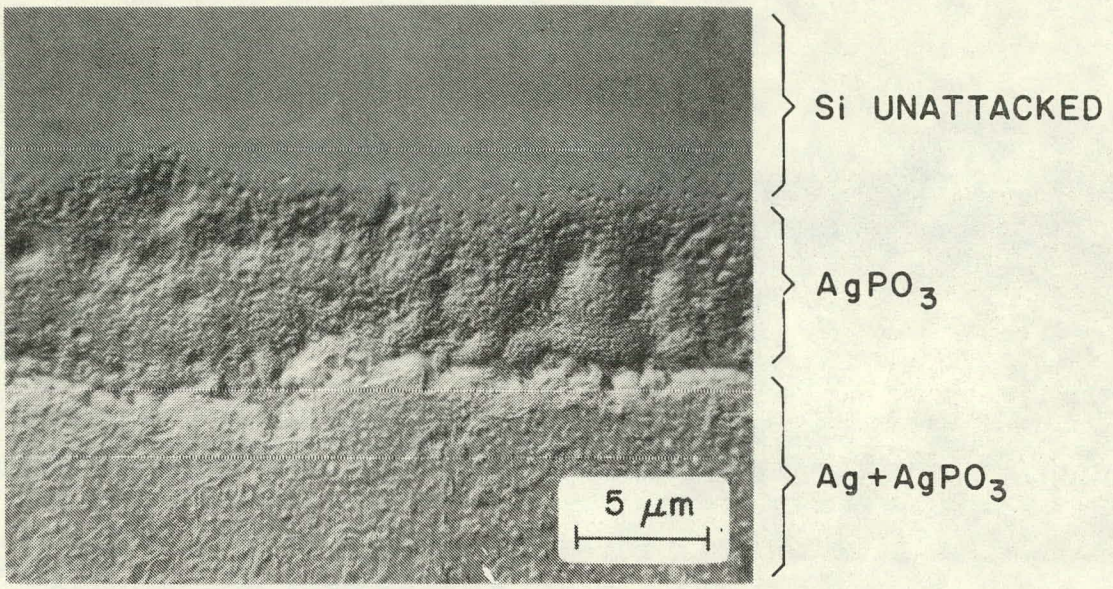

(a)

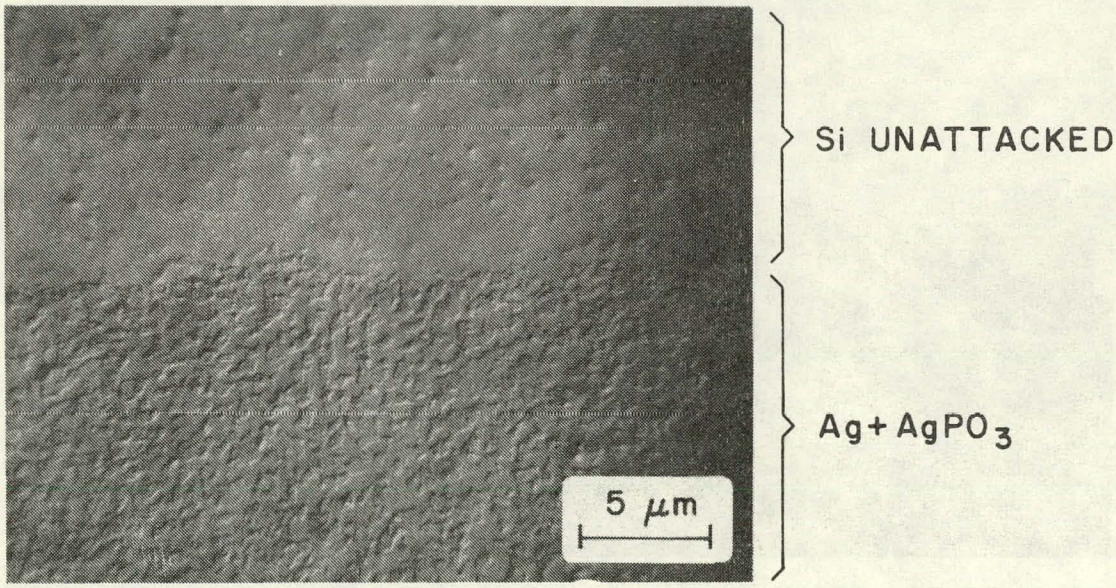

(b)

Figure 7. Metallized Si surfaces fired for 2 min at 650°C, Ag and $AgPO_3$ removed with etchants (Nomarski optics).
(a) (100) Si n-layer.
(b) (111) Si (100-Ω-cm resistivity).

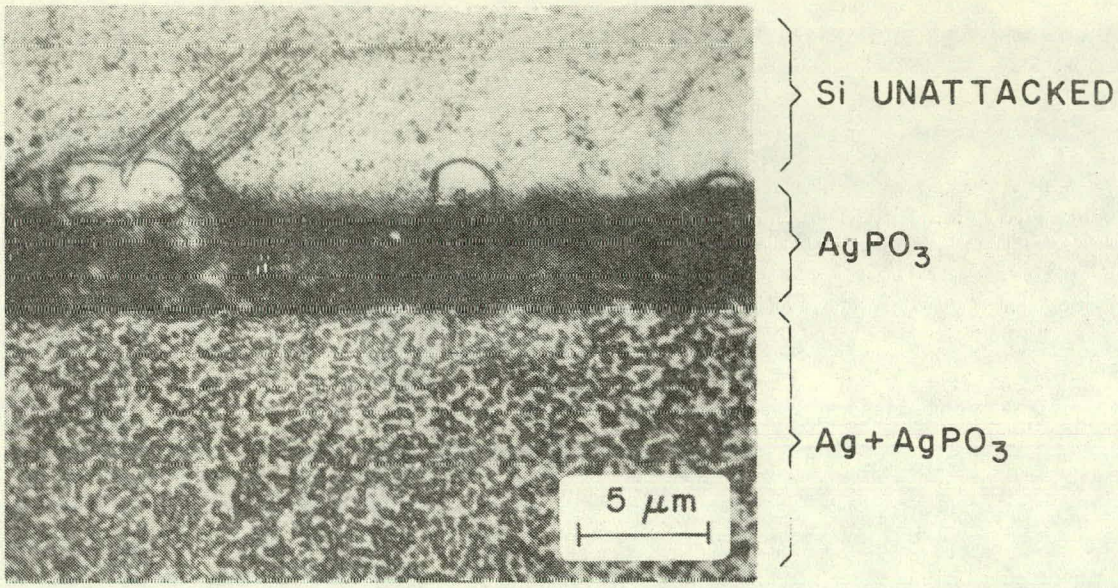

(a)

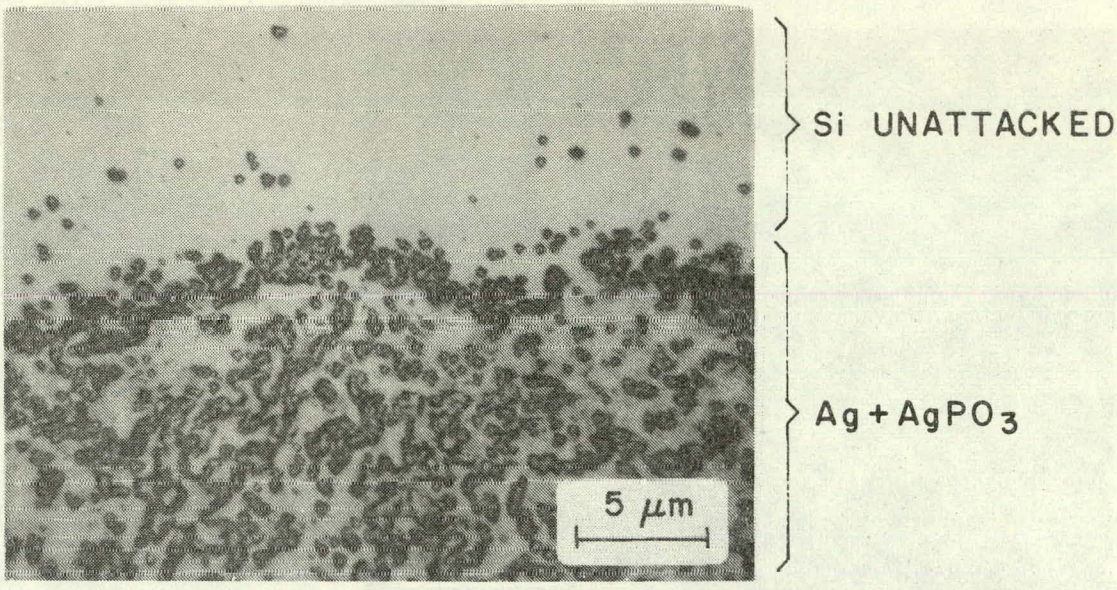

(b)

Figure 8. Metallized Si surfaces fired for 10 min at 700°C and $AgPO_3$ removed with etchants (Nomarski optics).
(a) (100) Si n-layer
(b) (111) Si (100-Ω-cm resistivity).

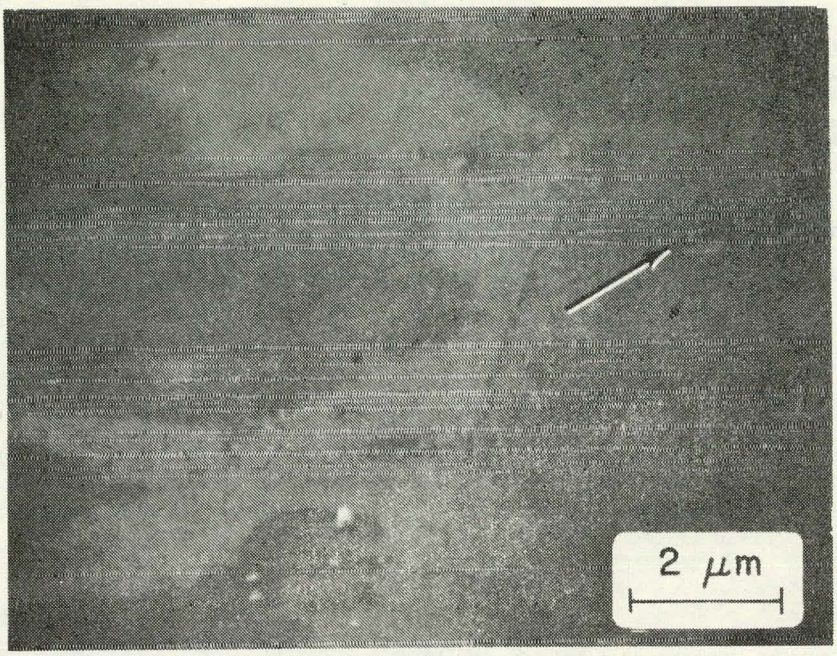

(a)

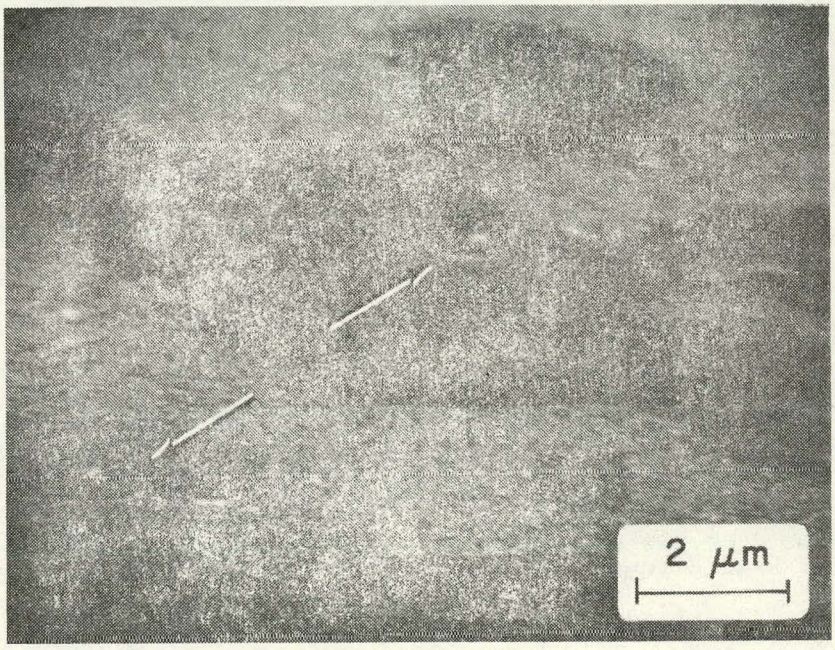

(b)

Figure 9. Metallized Si surfaces fired for 10 min at 700°C, Ag and $AgPO_3$ removed with etchants (SEM).
(a) (100) Si n-layer
(b) (111) Si (100-Ω-cm resistivity).

increasing the production rate. Initial tests with an Argus International* infrared lamp system appear to be providing adequate results with 1-min heating times as described below.

4. Solar-Cell Metallization

Preliminary experiments were conducted to test the use of infrared lamps for the firing of screen-printed solar cells. The test lot consisted of 40 3-in.-diameter solar-cell wafers with n^+ junction depths of ∿0.5 μm and sheet resistance of ∿30 Ω/□ formed by $POCl_3$ diffusion. This lot was split and printed on the sun-side with three different silver-based inks - Thick Film Systems - TFS 3347, RCA-Metz type C, and Englehard E-422E. The backs of all samples were printed with Englehard E-422F Ag ink containing 3 to 4% aluminum.

The firing tests were conducted using two Argus International #705 infrared lamp heaters. The samples were placed one at a time in a horizontal plane on a stainless steel grid belt and fired simultaneously from both sides. A thermocouple attached to the sun-side of the wafers indicated that a temperature of 775 to 800°C was achieved in 30 s. Experiments were conducted at firing times of 1/2, 1, 1-1/2, 2, and 3 min.

The results as a function of the firing time are shown in Table 7. Good results were obtained at all firing times as indicated by the maximum values shown in Table 7. However, wider variations in parameters were measured for the 30-s firing time, and some degradation in open-circuit voltage and short-circuit current is evident for increased firing time.

The solar-cell parameters as a function of ink are given in Table 8. It can be seen that the RCA type C ink yielded the best overall cell parameters with Thick Film Systems TFS 3347 a close second. The cells printed with Englehard ink E-422E generally had the lowest fill-factors, caused primarily by excessive series resistance.

The infrared lamp method of firing is rapid and seems to offer good stability and control. Further experiments will be conducted to assess the limits of this method and to determine optimum production parameters.

*Argus International, Hopewell, NJ.

TABLE 7. RESULTS OF INFRARED LAMP FIRING AS A FUNCTION OF FIRING TIME

Firing Time (min)	No. of Samples	AM-1 Parameters J_{sc}* (mA/cm^2)	V_{oc} (mV)	F.F. -	$F.F._{max}$ -	η** (%)	η_{max}
1/2	8	20.7	577	0.662	0.731	7.9	8.9
1	9	20.5	582	0.697	0.728	8.3	9.0
1-1/2	10	20.2	577	0.679	0.713	7.9	8.8
2	8	19.8	574	0.697	0.727	7.9	8.7
3	5	20.0	572	0.703	0.717	8.0	8.6

*Cell area = 39 cm^2
**No AR coating

TABLE 8. SUMMARY OF IR LAMP FIRED SOLAR CELLS AS A FUNCTION OF INK

Ink		Firing Time	AM-1 Parameters J_{sc}*	V_{oc}	F.F.	$F.F._{max}$	η	
Sun	Back	(min)	(mA/cm^2)	(mV)	-	-	(%)	η_{max}
TFS 3347	E-422F	1-3	19.8	577	0.690	0.713	8.0	8.8
RCA Type C	E-422F	1-3	20.4	582	0.700	0.717	8.2	8.8
Engelhard E-422E	E-422F	1-3	20.0	572	0.680	0.703	7.8	8.3

*No AR coating

C. ANTIREFLECTION COATING

1. Commercial Source Concentrate

As noted in ref. 2, we have used a commercial preparation (Silicatitania Film "C" by Emulsitone Co.) as a convenient source concentrate for our AR coatings. This preparation, of an undisclosed proprietary composition, forms a thin film when applied to silicon wafers by spinning. The dried film exhibits a refractive index of 2.0 to 2.1, making it suitable as an AR coating for silicon solar cells if a film thickness in the range of 700 to 800 Å is used.

We demonstrated that the preparation can be successfully deposited with good control by automated high-speed spraying, if it is properly modified with an organic agent of suitable composition, polarity, vapor pressure, surface tension, and viscosity. We had found that the key agent which renders this unexpected result feasible is 2-ethyl-1-hexanol.

2. Formulating Alternative Compositions for AR Coating Source Solutions

We consider it imperative to have full control over composition, materials purity, and supply of AR coating source materials. During this reporting period we designed several compositions that, on the basis of their chemistry, would be expected to yield AR films of appropriate refractive index for our specific application. Our systems are based on organometallic titanium and silicon alkoxides in a solvent base of alkyl esters and alkyl alcohols. The most promising systems, which on coating tests yielded films with properties similar to those obtained from the commercial preparation, consist of 1 volume titanium isopropoxide in 3 volumes of butyl acetate, with or without additions of ethyl acetate, isopropanol, acetic anhydride, and ethyl alcohol. Addition of silicon alkoxide is not required to obtain a refractive index of 2.1 (measured ellipsometrically with a helium-neon laser microbeam at a wavelength of 6328 Å). Lower refractive indices can be obtained by incorporating suitable quantities of tetraethylorthosilicate which forms SiO_2 ($n \sim 1.4$) on hydrolytic oxidation. A cost reduction by a factor of over 60 has been achieved by synthesizing this alternative source concentrate which yields films that are similar to those resulting from the commercial product, and which are adequate for our specific purpose. Dilution with 2-ethyl-1-hexanol makes it possible to use this preparation for automated spray deposition as previously reported for the commercial source concentrate.

3. Heat Treatment Effects

Controlled heat treatments of the air-dried film deposits are necessary for curing, stabilizing, and densifying the coating. The exact temperature and time of the heat treatment to attain optimal results is of considerable practical importance in large-scale processing, particularly the minimum time to achieve best results.

A matrix of experiments has been designed to assess the effects of heat treatments on films prepared from both the commercial and the in-house prepared AR coating source materials. Key properties being measured are film thickness, refractive index, absolute reflectance, and transmittance as a function of wavelength; the relative density by isothermal etch rate determination in $HF-H_2O$ etchants; structural perfection by Nomarski differential interference contrast microscopy and by SEM; and overall effects on solar-cell electrical performance. These studies are in progress at this time.

D. INTERCONNECT AND PANEL ASSEMBLY

1. PVB Lamination Process

It was clearly established that a temperature of 230°F or above is necessary to provide flow and extrusion of the polyvinyl butyral (PBV) across the cell face and into the void between the cells. At 230°F the PVB is soft, but substantial pressure is necessary. At 275°F, the PVB flows readily with moderate pressure.

Successful lamination requires a minimum of air between the layers of glass, PVB, and silicon cells. Small amounts of residual air are dissolved into the PVB by high hydrostatic pressure ($\sim$150 psi) and temperature (275°F), over a period of 30 to 60 min. If too much air is entrapped between the cells, however, it will not dissolve, and bubbles remain. This will cause delamination later in the life of the panel.

Therefore, it is necessary to define a process that first applies a partial vacuum to the layup (consisting of glass-PVB-cell-PVB-glass), then applies a low hydrostatic pressure on the surface of the glass plates together with moderate temperature (obtaining partial flow of PVB), and then the full hydrostatic pressure and temperature. The reason for the intermediate pressure/temperature schedule is to avoid sealing off the air passages as long as possible by minimizing the amount of tack and self-sealing of the two layers of PVB.

A vacuum bag, enclosing the layup, is used to allow simultaneous vacuum and pressure to be applied inside a laminating autoclave. This technique is well established in the safety glass industry for laminating glass sandwich that cannot be handled by pressure rollers. The bag allows a vacuum to be maintained between the glass layer while simultaneously pressurizing the glass sheets externally.

A typical laminating schedule (not necessarily optimized) is shown in Fig. 10. Various thicknesses of PVB, types of cells, and manufacturers of PVB were tried. PVB thicknesses were 0.30 in. (2 layers) and 0.015 in. (2 layers). Monsanto* (ribbed surface) and DuPont** (orange peel surface) PVB were compared for effectiveness in removing air. Due to cell availability, solid copper and silicon-only dummy cells were used for most of the experiments, except for live cells in the 4- by 4-ft panel described below. In all cases, the cell configuration was that of a working panel, including bus bars.

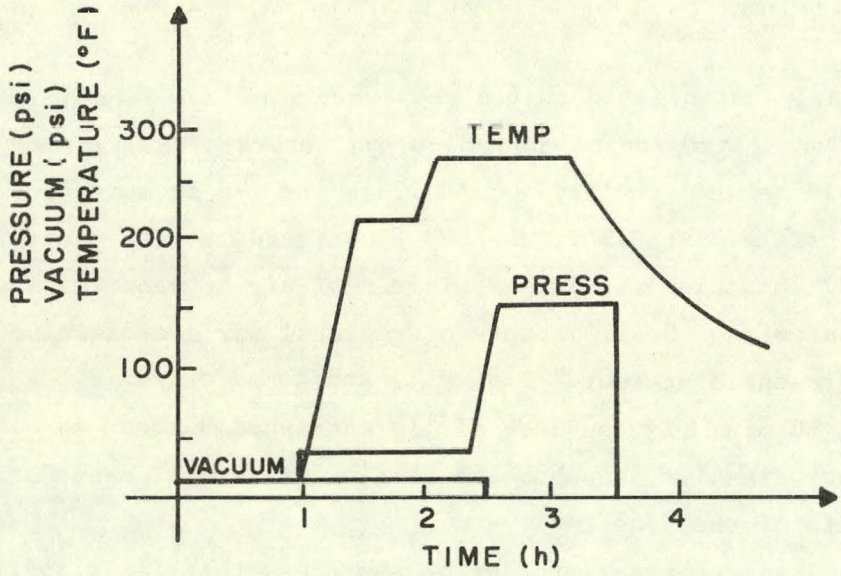

Figure 10. Lamination schedule.

a. Copper Cells - These dummy cells appear to cause sufficient thermal stress to break the glass panel during or after cool-down. We have not had success at laminating panels with these cells. Panels have been observed to crack spontaneously shortly after the laminating process. Therefore, these cells cannot be used as mechanical substitutes.

b. Silicon Cells - Silicon cells, on the other hand, do not appear to cause excessive thermal stress. Even though several samples have retained bubbles, the glass itself has generally remained intact. Breakage of the glass has

*Monsanto Co., St. Peters, MO.
**du Pont de Nemours & Co., Inc., Wilmington, DE.

been traced to other causes, such as solder spikes and similar inclusions that cause local stress concentration.

The silicon cells themselves have rarely broken during the lamination process. When properly scheduled, the pressurization appears to be sufficiently gentle to preclude breakage due to localized bending of the cells across a properly soldered interconnect. Occasionally, two cells have overlapped at their tangent point, in which case fracture occurred due to edge shear. Proper fixturing during manufacture would preclude this.

One string of live cells (14 cells) was included in a 4- by 4-ft panel. Output of the string after lamination was commensurate with individual I-V measurements prior to laminating. Detailed correlation has not yet been made.

Figure 11 shows the large panel that was successfully laminated. The panel measures roughly 40 by 45 in. (using 3-in.-diam cells) and is wired as 5 parallel strings of 43 cells in series. Because the available cells are smaller than would ultimately be used, additional series cells were added to approach a 48-in. dimension. Results also settle the question of scale effects. This panel is bubble-free and crack-free, except for a small front-side crack defect due to an external foreign particle.

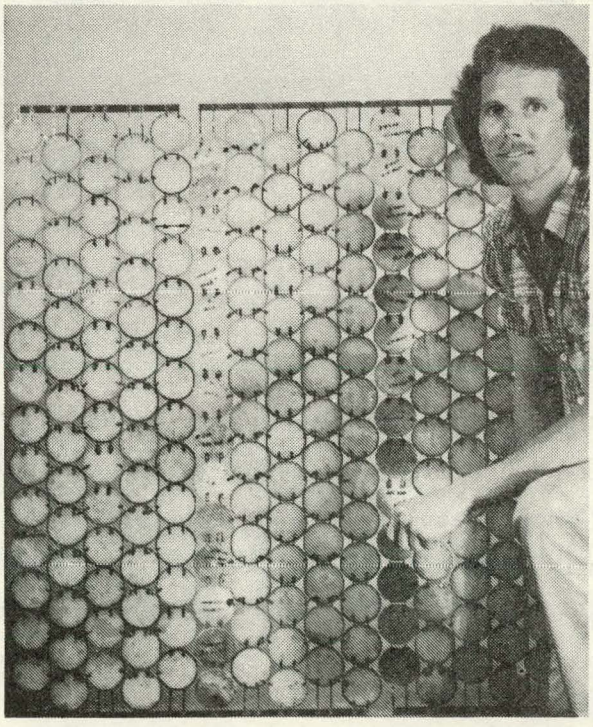

Figure 11. 40- by 45-in. laminated solar panel (backside).

An unsuccessful lamination can be seen in Fig. 12, where the effect of air entrapment is shown. In this case, the panel was evacuated and the pressure increased to approximately 30 psi in the autoclave, and the temperature raised to 210°F. Then the panel was removed for inspection. Although some flow of PVB had occurred, substantial voids remained, and repressurization and heating to maximum values failed to re-expel the air. This result emphasizes the requirement of obtaining and maintaining a good vacuum until late in the cycle, when flow is complete.

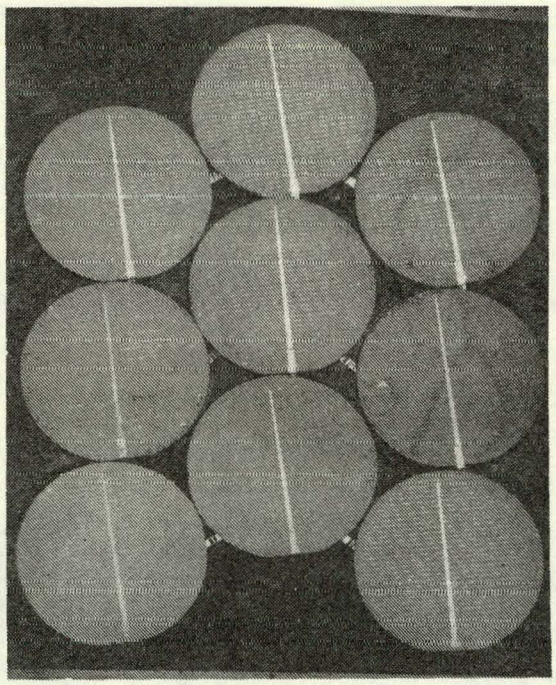

Figure 12. Lamination defects.

2. Acrylic Lamination

Approximately 30 small experiments were run (up to 18- by 12-in. panels) with varying mixtures of butyl/methyl methacrylate monomers, catalysts, and curing temperatures. Best results to date have been with a 60% butyl acrylate/methyl methacrylate mix, using 67% t-butyl-peroculate catalyst, at approximately 65 to 75°C oven cure. Some of these experiments have been cured slowly lowering the panel into a hot water bath at 90 to 95°C which produces a moving boundary of cured/uncured material.

The primary difficulty encountered in all of the experiments is the appearance of bubbles in the cured polymerized mix. The bubbles are due primarily to nonuniform shrinkage during the curing process. Inasmuch as the material shrinks 20% when passing to the polymerized state, a constraint on the boundaries of a fluid element (as imposed by the glass plates) will produce an elastic stress sufficiently high to result in formation of a void. If the material were to cure with absolute uniformity, then the shrinkage itself would be uniform and the stress would not be produced. This was demonstrated by curing the monomer mix under identical conditions, but using a sheet of polyester on one side rather than glass.

By thermally creating a moving boundary between cured and uncured material, the uncured monomer can flow into the shrinking polymer in the boundary zone, hence minimizing locked-in stress. Several castings were produced bubble-free by this method. The process, however, requires a long time cycle: dip rate was between 1 and 6 in./h at approximately 85°C.

In order to position the cells midway between the glass plates, uncured polysulfide "dots" are deposited on the back of each cell (of an interconnected array), and one sheet of glass is then pressed onto the array of cells so that the polysulfide attaches the cells to the glass at a given spacing from the glass. The second (front) sheet of glass is assembled to the first, using a polysulfide seal around the perimeter together with spacers to provide proper separation. The panel is then heat cured and filled with monomer and cured.

It was found that a relatively large "dot" in the center of each cell caused breakage of the glass panel after the final cure, apparently due to differential expansion of the polysulfide vs acrylic materials. Use of three small dots avoided this problem. This method of mounting cells is directly amenable to high-volume production. The two methods are shown in Fig. 13.

To date, we have not been successful in producing a cast panel that remains bubble-free when heated to the upper environmental temperature of 95°C for several days. The mechanism of bubble formation during post-cure heating is as yet unexplained.

Limited preliminary testing between -40 and +95°C has been done on both PVB and acrylic samples. While the acrylic cast samples show bubble formation as noted above, the PVB panels do not show any tendency to form bubbles or delaminate.

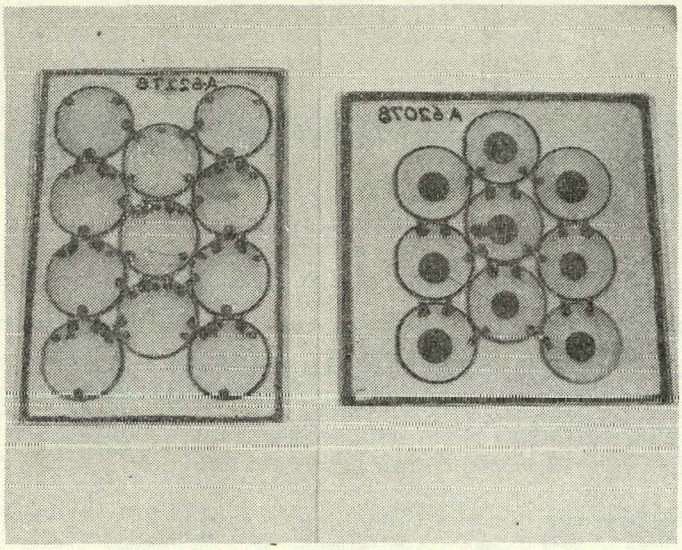

Figure 13. Method of mounting cell array for acrylic coating.

3. Radiant-Heat Mass-Soldering Technique

Methods were investigated by which an entire array of solar cells could be electrically interconnected in a single "mass-soldering" process. In the initial concept the pretabbed cells are arranged in the desired configuration, clamped between a silicone sponge rubber pad and an aluminum plate, and conductively heated by a hot plate. However, there are some drawbacks to this method. When the low-cost screen-printed silver/glass frit metallizations are soldered, reflowing temperature and time must be minimized to avoid dewetting of the silver from the glass frit which degrades the electrical contact and weakens the mechanical bond. The conductivity-heated mass-soldering method has the disadvantage of lengthy heat-up and cool-down times. This is due to the large thermal mass of the aluminum plate, which must be thick enough to be sufficiently rigid to clamp all the cells in place. Also plate warpage severely reduces conduction contact area between the hot plate and soldering fixture. For this reason, radiant coupling of the same soldering fixture was pursued. This, however, resulted in even longer heat-up times.

From this, a new concept evolved wherein the cells are heated directly by radiant heat, eliminating the large thermal mass of the aluminum clamping platen. The initial radiant mass-soldering fixture (see Figs. 14 and 15) consists of a

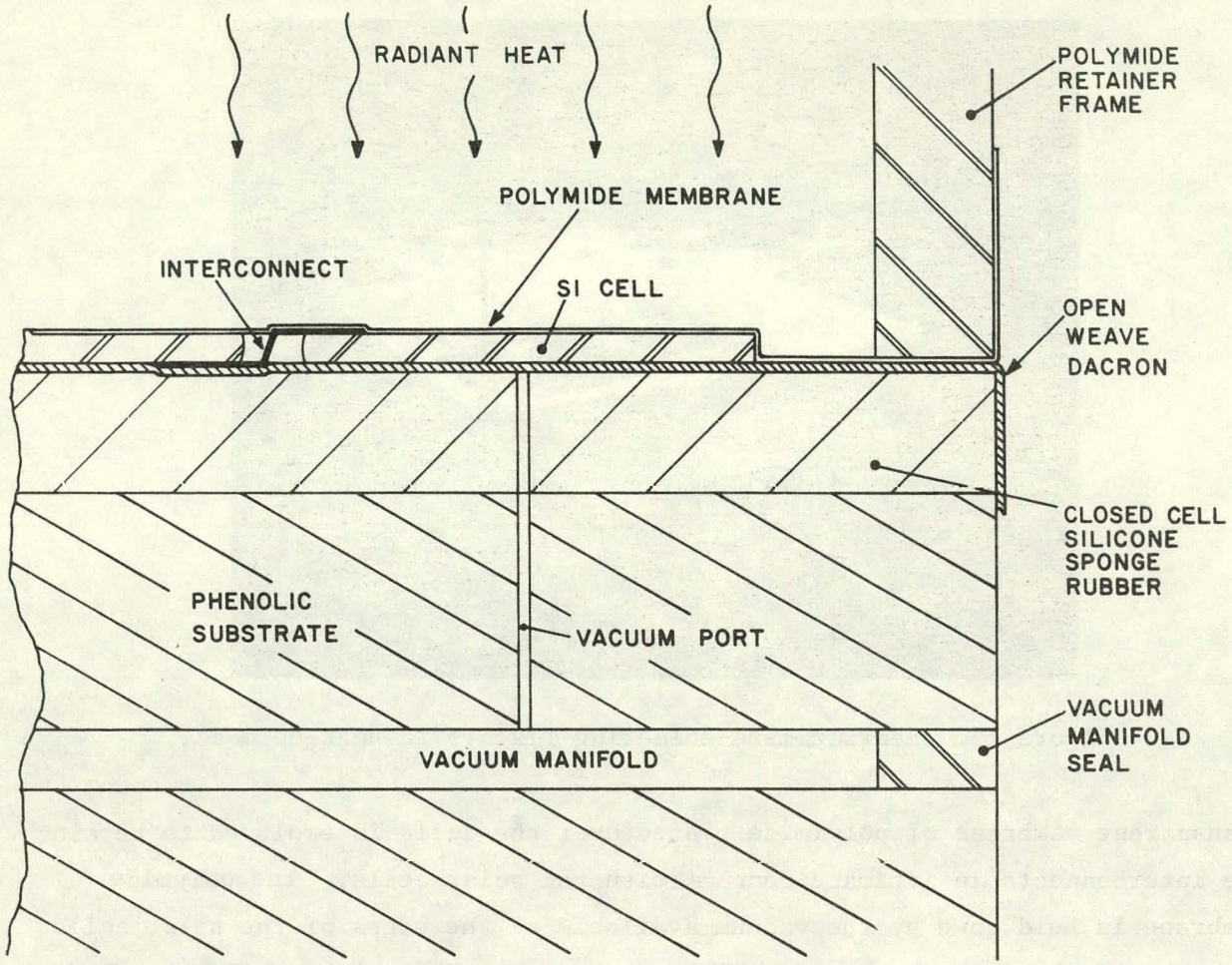

Figure 14. Section view of edge of radiant mass-soldering fixture.

1-ft^2 vacuum platen with a 1/4-in.-thick pad of close-celled silicone rubber adhered to it, which reduces heat conduction out of the cell. The 9 cells are held in place by a vacuum port located beneath the center of each cell. A thin layer (1 to 2 mil) of open weave material is located between the silicone sponge rubber and the solar cell which acts to spread the vacuum evenly over the entire area. This material must be able to survive the soldering temperature (~200°C) and also resist wetting by the molten solder. Dacron,® stainless-steel mesh, and aluminum mesh are candidate materials for this application. A thin

®Registered trademark of du Pont de Nemours & Co., Inc.

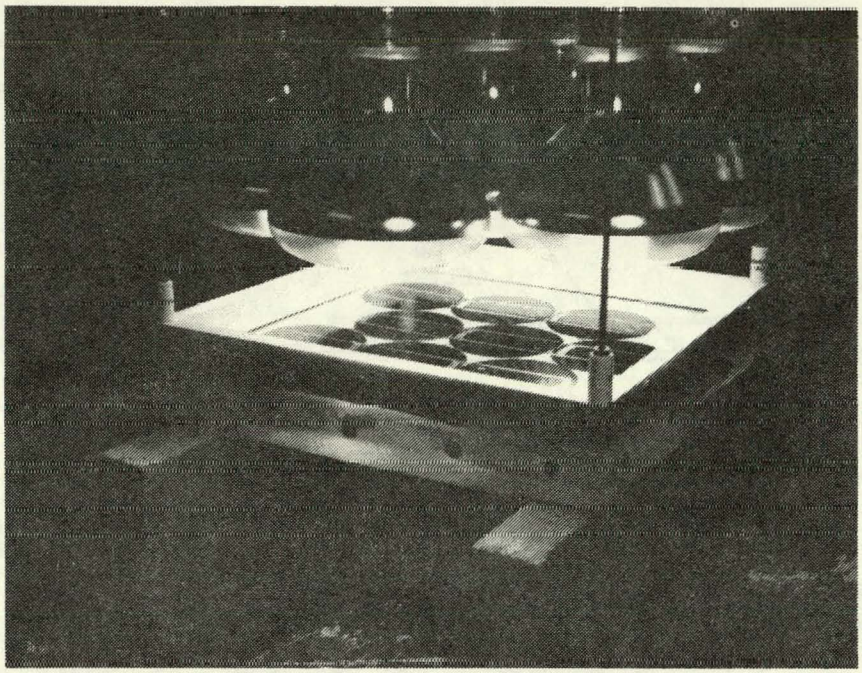

Figure 15. Radiant mass-soldering fixture in heat-up mode.

transparent membrane of polyimide placed over the cells is employed to retain the interconnects in intimate contact with the solar cells. The polymide membrane is held down by the vacuum available at the edges of the solar cells by means of the open weave material beneath them. The polymide is stretched over a frame which forms the edge seal for the vacuum. The radiant absorption of the yellow transparent polymide results in a 7.5% increase in the time it takes to raise the temperature of an AR-coated silicon cell from ambient to 200°C when compared with no membrane. This method of retaining the interconnects in contact with the solar cells results in smooth, flat solder joints; further, the method has distinct advantages over that used in the conductive fixture in that the clamping pressure is uniform and can be regulated by the level of the vacuum employed and that the cell is being clamped down against a compliant substrate. This can be best appreciated in light of the fact that several arrays reflowed in the conductive fixture were ruined by cell breakage due to small solder lumps left after the tinning and pretabbing operations. When the cells are clamped between the silicone sponge rubber and the aluminum

platen, the cells are deflected over these solder lumps resulting in cell breakage. Therefore, the radiant mass-soldering fixture will furnish a greater throughput.

The radiant heat source used consists of an array of seven 375-W reflector type heat lamps arranged in a close-packed hexagon. It was empirically determined that the radiant flux is uniform at a distance of 2.75 in. from the top of the lamps. At this distance an AR-coated silicon cell 15 mil thick was heated from ambient to 200°C in 45 s, compared with over 4 min for the conductive soldering fixture. This short duration reflowing process not only ensures superior quality joints but also greatly reduces the amount of energy expended per array and therefore reduces panel cost. The importance of the AR coating in absorbing heat is exemplified by the fact tha a nonAR-coated cell takes more than five times longer to reach 200°C. To implement this method as a continuous process for production, it has been proposed that the solar-cell array be traversed beneath an array of heat lamps, 4-ft^2 at a rate of one soldered array every 45 s.

SECTION IV

PLANS FOR THE NEXT QUARTER

A. JUNCTION FORMATION

1. Ion Implantation

The following tests and experiments are planned or are in progress:

(1) Test for starting wafer quality and origin. A matrix of 60 samples will be run using starting wafers of four different types listed below:

Vendor	Wacker*	Monsanto	Monsanto	Monsanto
Resistivity (Ω-cm)	1-2	1-2	8-12	0.5-2
Crystal	FZ	CZ	CZ	CZ
Surface	Polished	Etched	Polished	Etched

The starting wafer diffusion lengths have been measured (SPV method) and will be measured again after processing. All wafers will be implanted with ^{31}P with a dose of 5×10^{15} A/cm^2 at 5 keV. Half the wafers will be gettered by the three-step method and half by the boron-glass technique.

(2) Test for ^{31}P implant energy level from 5 to 50 keV.

2. Liquid-Dopant Sources

Tests will be made to determine the feasibility of a roll-on or screen-on process for aqueous-base phosphorus sources. The quality of junctions and solar cells found will be studied.

*Wacker Chemical Corp., Richardson, TX.

B. SCREEN-PRINTED METALLIZATION

Experiments are planned to test the limits and to determine optimum processing parameters for infrared-lamp firing. These tests will be conducted on solar-cell lots of fixed junction depth. RCA, Metz type-C, and Thick Film Systems 3347 will be used. Also, firing from the top and simultaneous top/back firing will be assessed.

We will determine the sensitivity to n-layer junction depth with a more complete characterization of metallization penetration.

Additional testing will be done with RCA synthesized ink by varying the Ag-$AgPO_3$ concentration.

Diagnostic electrical measurements will be performed and analyzed comparing screen-printed solar-cell lots with cells metallized with evaporated Ti/Ag.

C. SPRAY-ON ANTIREFLECTION COATING

Our plans for the next quarter include the following:

(1) Complete the heat treatment studies of AR coatings and define optimum processing conditions.
(2) Devise masking or etching techniques to permit contacting the metallization bonding area of AR-coated solar cells.
(3) Deposit RCA synthesized AR coatings by optimized automatic spray deposition on metallized solar cells and evaluate the effects on electrical performance of the cells.
(4) Characterize optical, chemical, and physical properties of AR films formulated and deposited at RCA.
(5) Describe the results of the AR coating studies in a second and final technical report which will include details of the recommended processing procedure.

D. SOLDERING TECHNOLOGY

The interconnect retainer membrane and compliant insulated substrate will be optimized to reduce heat-up time and to also provide long maintenance intervals. Also the optimum open weave vacuum spreader material will be

determined. Once the materials are optimized, the prototype will be enlarged to enable mass soldering a 4-ft^2 array.

E. PANEL ASSEMBLY

1. PVB Lamination

Two more panels are planned (4 x 4 ft); one will be load tested to determine structural strength, and one will be thermally cycled. Two smaller panels will be fabricated with the live solar cells for demonstration and further experiment.

2. Acrylic Casting

Castings will be made with the acrylic monomer under vacuum conditions to determine if re-solution of air during pouring is the source of bubbles. A large panel will be cast to demonstrate feasibility of the method for production of full sized units.

3. Cost Estimate

A factory production cost estimate will be obtained for the PVB process in large volume production.

APPENDIX

DETECTION OF MICROCRACKS IN SILICON WAFERS

1. Introduction

It is conceivable that the forces involved in screen-printing operations for depositing the metallization grid could introduce latent or actual defects in the silicon substrate crystal, particularly in the case of silicon wafers containing stress-raising flaws introduced by the ingot sawing operation. To settle this question, two analytical techniques were applied for the purpose of detecting such defects: (1) nondestructive decoration of actual microcracks with fluorescing dyes and (2) chemical etching of the silicon to detect latent microcracks and surface irregularities. The solar-cell wafers that had been subjected to a test of worst-case screen-printing conditions followed by thermal shock cycling from -196 to 200°C, as described on page 26 of Quarterly Report No. 2 [2], were analyzed by these techniques. As was noted, no cracks were present. However, the sensitive analytical techniques we developed specifically for this test purpose are described since they are generally applicable to similar testing requirements.

2. Nondestructive Detection of Microcracks by Fluorescent Dye Penetration and Decoration

Silicon samples with artifically induced cracks were used as test vehicles. The samples consisted of single-crystal silicon wafers, lapped on one side and polished on the other, on which a 1-μm-thick SiO_2 layer was thermally grown.

The principle of the test method is the introduction of a UV-fluorescent dye solution into the microcracks. This is accomplished by applying the dye solution containing a penetrating agent over the entire surface of the thoroughly cleaned test sample. Capillary action draws the liquid, of optimal viscosity, into the cracks or any other discontinuities. A dwell or set time of a few minutes is allowed before the surface is sprayed with an appropriate solvent which removes most of the test solution except that which remains in the depressed defects. Some of the dye solution from the defects may deposit near the defect site during drying. The dried sample

is then inspected under the microscope during intense UV irradiation. Cracks and recessed flaws show up in sharp contrast to the surrounding surface.

A UV photomicrograph of a decorated test sample (SiO_2 film on polished silicon) is shown in Fig. A-1. During microscopy, the microcrack is clearly visible as a bright green fluorescing line (seen as white in black background in the 150X photomicrograph). On a smooth sample, surface microdroplets of intensely fluorescing solution have redeposited and surround and decorate each defect so that even extremely small defects are readily demarcated. On a rough surface (such as a sawed or lapped silicon wafer) a few microdroplets remain, but the cracks show up clearly as bright fluorescing lines in a basically dark background.

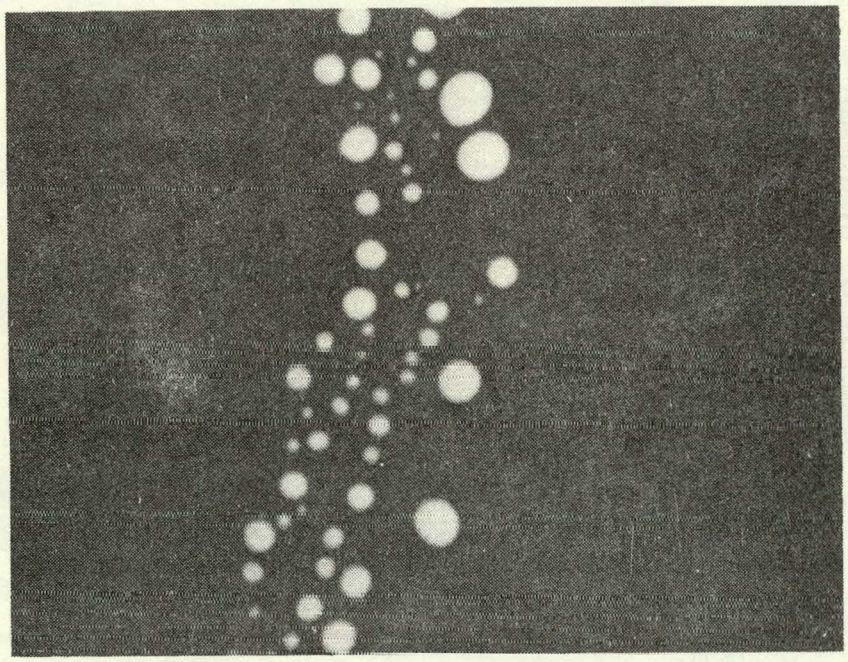

Figure A-1. Photomicrograph under long-wavelength UV irradiation showing microcrack containing fluorescent dye penetrant solution surrounded by redeposited decorating microdroplets of the fluorescent dye solution. (150X).

The reagents we selected for this sensitive test are P-133A Zip Tracer Tech penetrant fluorescing dye solution, and K-410A removing solvent; both are available commercially in spray cans from Uresco, Inc.* A pair of

*Uresco, Inc., Downey, CA.

pencil-type, low-pressure, mercury discharge, long-wave UV lamps mounted just above the stage of a Reichart research microscope served as the radiation source for observation of the decorated samples.

3. Chemical Etching Techniques for Detecting Latent Microcracks and Surface Flaws

The fluorescent dye penetration test described above is excellent for detecting distinctly recessed discontinuites. Subsurface cracks, buried or latent crystal defects, and shallow surface irregularities such as saw marks are not detectable by this method. Therefore, chemical etching techniques were developed and optimized as a complementary method that is capable of detecting these types of defects.

The isotropic etchants used consisted of a freshly prepared mixture of 5.0 vol HNO_3 70% - 3.0 vol HF 49% - 3.0 vol CH_3COOH 99%, with and without 0.1% of a fluorocarbon surfactant (FC-93 Fluorad, 3M Company). Etching was performed with agitation at room temperature and was terminated by diluting the etch solution with water. The test samples were sawed; (100)-plane silicon wafers of 7.5-cm diameter are used as substrates for solar-cell fabrication. Apiezon wax was used as an etch mask to produce a pattern of stripes across the wafer surface. A Talysurf and a Tencor stylus profilometer were used to measure the etch depth and the surface morphology.

The etchant without surfactant etched at a rate of 1.1 μm/s and produced a mirror finish, but only after a minimum of about 50 μm was etched off each side. Defects in the crystal showed up clearly, and any microcracks and shallow subsurface cracks if present would have been enlarged by the etching action and become clearly visible. Surface defects became clearly demarcated on the etch polished surface. For example, entire arrays of circular groove marks measuring 150 μm per groove and up to several micrometers in depth became distinctly discernable by the naked eye when viewed in reflected white light.

The etchant containing the surfactant as penetrating agent etched at the same rate but produced a uniform satin finish due to the formation of microscopic nodules, as shown in Fig. A-2, rather than the mirror polish obtained with the surfactant-free polishing etch. We did not find any advantage for analytical testing applications of this etchant; in fact, the surface morphology features after etching were not as easily seen as with the mirror smooth polish of the surfactant-free composition. However, the micronodular surface resulting from the isotropic surfactant etch may be of interest for chemical texturing of the silicon surface to reduce the reflectivity of incident light.

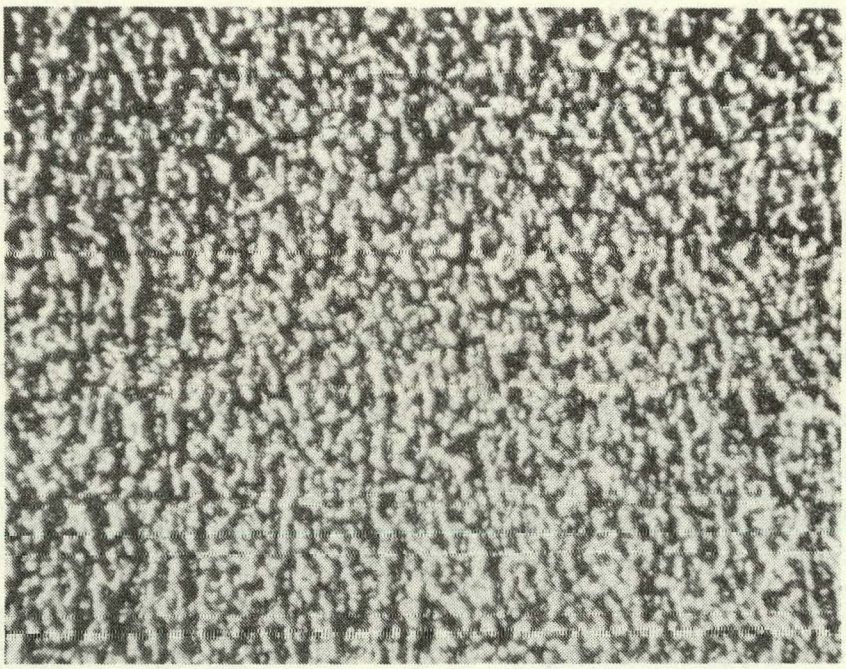

Figure A-2. Photomicrograph (40X) of silicon surface etch-textured to a nodular finish of low reflectivity satin appearance. Silicon: (100)-plane, 1 to 5 Ω-cm p-type, sawed wafer (No. 4), as used for solar-cell fabrication. Etchant: HNO_3(70%)-HF(49%)-CH_3 COOH(99%), 5:3:3 by volume, containing 0.10% FC-93 fluorocarbon surfactant. Etching: 60 s at 25°C with agitation removing 62 μm from sawed surface.

*U.S. GOVERNMENT PRINTING OFFICE: 1979-640-014/4014. Region 4.